https://dx.doi.org/10.21577/0103-5053.20220146

J. Braz. Chem. Soc., Vol. 34, No. 6, 778-784, 2023

Article

Synthesis and Characterization of Au@MnO_2 Nanoparticles as Plasmon Enhanced Spectroscopy Substrates

Gabriela P. Oliveira,[a] Tatiana B. V. Neves,[a] Linus P. F. Peixoto,[a] Sandra M. Landi,[b] Bráulio S. Archanjo[b] and Gustavo F. S. Andrade[,a]*

[a]*Laboratório de Nanestruturas Plasmônicas, Núcleo de Espectroscopia e Estrutura Molecular, Centro de Estudos de Materiais, Departamento de Química, Universidade Federal de Juiz de Fora, R. José Lourenço Kelmer s/n, Campus Universitário, 36036-900 Juiz de Fora-MG, Brazil*

[b]*Divisão de Metrologia de Materiais, Instituto Nacional de Metrologia, Qualidade e Tecnologia (INMETRO), Av. Nossa Senhora das Graças, 50, Prédio 3, 25250-020 Duque de Caxias-RJ, Brazil*

The plasmonic properties of Au nanoparticles (AuNP), which allow the observation of enhanced spectroscopic effects, are strongly affected by the aggregation and precipitation caused by the strong interactions between nanoparticles. To avoid AuNP aggregation and precipitation, the present study proposes coating with MnO_2, forming AuNP@MnO_2 core-shell structures. The MnO_2 layers presented 1-10 nm thickness so that highly surface-enhanced fluorescence was obtained with maximum intensity given by 5 nm thick MnO_2. The decrease in Raman intensity could be controlled, despite the inherent reduction in surface-enhanced Raman scattering (SERS) intensity with increasing adsorbate-surface distance. The decrease in Raman intensity was compensated by increasing AuNP stability caused by the MnO_2 shell.

Keywords: SHINERS, SHINEF, manganese oxide, IR-820, Au nanoparticles

Introduction

The localized surface plasmon resonance (LSPR) may be characterized by the excitation of collective electron oscillation on metallic nanostructure surfaces by an exciting resonant radiation. LSPR occurs in the visible or near-infrared region for specific metals, such as Ag, Au, Cu, and alkaline metals.[1] The frequency of the LSPR strongly depends on the size and shape of plasmonic nanostructures and the dielectric environment in which the plasmonic nanostructures are immersed.[2]

Specifically, when the refractive index increases in the vicinity of the nanoparticles, there is a displacement of the LSPR band to lower energies, usually referred to as a red shift; additionally, variations in the intensity and bandwidth may also occur.[3,4] Following the changes in the LSPR band position during a deposition process on plasmonic nanostructure is, thus, an efficient way of evaluating surface changes in those nanostructures.[5]

The collective electron excitation in LSPR significantly increases the local electromagnetic field in the immediate surroundings of plasmonic metal nanostructures. This enhancement of the electric field mainly allows the occurrence of plasmon-enhanced spectroscopic phenomena such as surface-enhanced Raman scattering (SERS) and surface-enhanced fluorescence (SEF).[6,7] SERS and SEF have been developed over the years to be applied in several areas, such as analytical chemistry,[6-9] biodiagnostics,[10-12] and materials science.[13-15]

One major issue for plasmon-enhanced spectroscopies is the observation that nanoparticles of coinage metals (Au, Ag and Cu) interact strongly with each other and may form aggregates in suspension, which strongly affects both suspension stability and spectroscopic characteristics reproducibility. In this context, the shell-isolated nanoparticle (SHIN) substrates emerged aiming to minimize the aggregation effects.[16] SHIN substrates are comprised of nanoparticles covered by oxides, usually dielectric or semiconductors, such as silicon oxide; these core-shell nanostructures may preserve most of the plasmonic properties of the coinage metals and present the surface properties of the shell oxide. The initial proposition of SHIN resulted in increased interest in the importance of core-shell nanostructures for application in plasmon-enhanced spectroscopies in the last years due to

*e-mail: gustavo.andrade@ufjf.br
Editor handled this article: Jaísa Fernandes Soares

the possibility of combining varied materials in core and shell and obtaining many unique properties.[17]

The derived techniques SHINERS (shell-isolated nanoparticles enhanced Raman spectroscopy) and SHINEF (shell-isolated nanoparticles enhanced fluorescence) thus, arose to obtain enhanced spectroscopy substrates with increased stability and presented the additional characteristics of avoiding direct contact between the adsorbate and the metallic surface.[18] Both techniques have their performance modulated by the thickness of the dielectric layer, which separates the metallic surface of the molecular probe.[19] For SHINERS, the increase in the thickness of the dielectric layer causes a decrease in Raman intensity of the molecular probe due to the increasing distance between the probe and the surface, so there is usually a trade-off between improved stability and SHINERS performance.

In SEF, the direct contact between fluorophore and metal suppresses fluorescence due to coupling with surface plasmon, resulting in energy flow from fluorophore to metal competing with fluorescence.[20] This occurrence results, for SHINEF and thinner layers, in an increase in fluorescence intensity with thickening of the dielectric layer, which is the result of decreasing the suppression caused by the metal surface conjugated with the LSPR-enhanced local electric field. The increase in fluorescence intensity tends to reach a maximum value for an optimal thickness because both the decrease in suppression and the LSPR enhanced field become less important for thicker layers.[21]

For both SHINERS and SHINEF methodologies using a suspension of core-shell nanoparticles and the molecular probe, the signal enhancement may be evaluated by the AEF (analytical enhancement factor), equation 1. AEF is the simplest way of calculating enhancement factors because it is a simple relationship between the intensities in the enhanced spectroscopies (both SERS/SHINERS and SEF/SHINEF) and the non-surface-enhanced spectra at some given concentration, with the experimental care of keeping the spectral conditions constant.[22] AEF is well known to underestimate enhancement factors, as the relationship cannot account for the molecules that are not close enough to the surface to present an enhancement of spectroscopic events.[22,23] Still, the method allows grasping the enhancement factor trend during materials optimization.

$$AEF = \frac{I_{SE} / C_{SE}}{I_{NE} / C_{NE}} \quad (1)$$

In equation 1, I_{SE} is the intensity in the surface-enhanced (SE) spectra (SERS, SHINERS, SEF, or SHINEF), C_{SE} is the concentration of the probe molecule used to obtain the SE spectra, I_{NE} is the non-enhanced spectra (either Raman or fluorescence) of the molecular probe and C_{NE} is the concentration of the molecular probe used to obtain the non-enhanced spectra.

Among the oxides that have been used to develop SHIN materials, manganese dioxide, MnO_2, can be used as the shell layer of Au nanoparticles core plasmonic material, as it has been shown by Lin *et al.*[24] The results of the authors indicated that the MnO_2 thickness might be controlled by the initial concentration of potassium permanganate used as the manganese source. MnO_2-covered Au nanoparticles (Au@MnO_2) kept their plasmonic absorption with a red shift proportional to MnO_2 layer thickness. MnO_2 is a semiconductor material that has low cost, low toxicity, and abundant storage, and is insoluble in strongly alkaline medium, differently from other usual SHIN layers such as SiO_2 and Al_2O_3.[24,25] It has recently been shown that gold nanorods may be modified by manganese oxide, resulting in compact layers of the oxide, which could be used as SHINEF and SHINERS substrates.[26]

Au@MnO_2 may present a relevant potential for applications, such as catalysis and fluorescence sensing. Recently, Zhou *et al.*[27] used the catalytic reduction of 4-nitrophenol to aniline for the degradation of methylene blue and fluorescence sensing of glutathione. Ag@MnO_2 was used by Abdulrahman *et al.*[28] to detect methyl parathion on the surface of an orange fruit, concluding that nanoparticles were stable in an alkaline medium and that they were efficient SHINERS substrates.

In the present study, MnO_2-covered Au nanoparticles (Au@MnO_2) were obtained by controlling the oxide shell thicknesses over AuNPs, avoiding reagent excess; the manganese oxide coverage was characterized using LSPR, transmission electron microscopy (TEM), energy-dispersive X-ray spectroscopy (EDS), and scanning transmission electron microscopy high-angle annular dark-field (STEM-HAADF) chemical imaging. The resulting Au@MnO_2 nanoparticles were applied as substrates for two surface-enhanced spectroscopies, SHINERS (λ_0 = 633 nm) and SHINEF (λ_0 = 785 nm), by choosing the best layer thickness of each technique, using the same probe molecule, the cyanine dye IR-820.

Experimental

Chemicals

Tetrachloroauric acid ($HAuCl_4$, 99%), trisodium citrate (Na_3-cit, 99%), potassium hydroxide (KOH, 85%), (3-aminopropyl)trimethoxysilane (APTMS, 97%), sodium oxalate ($Na_2C_2O_4$, 99.5%) and the probe molecule IR-820

(80%) were all acquired from Sigma-Aldrich (Darmstadt, Germany), potassium permanganate ($KMnO_4$, 99%) from Vetec (Duque de Caxias, Brazil), and used without any further purification. All aqueous solutions have been prepared using deionized water (resistivity = 18.2 MΩ cm) from a Millipore (Darmstadt, Germany) Synergy UV system.

Synthesis of AuNPs

The gold nanoparticle suspensions (AuNP) have been synthesized from the precursor $HAuCl_4$ in an aqueous solution using Na_3-cit as a reducing agent following the well-known procedure proposed by Frens.[29] Briefly, 50 mL of an aqueous 0.01% m/v $HAuCl_4$ solution were brought to boiling under reflux, followed by the addition of 500 or 1000 μL of a 1.0% m/v Na_3-cit solution. The boiling was maintained for about 5-10 min until the suspension acquired the characteristic red color.

Synthesis of Au@MnO_2

The AuNP presented 16 and 50 nm as average diameters. For AuNP (50 nm), the procedure was described by Lin *et al.*[24] for the MnO_2 thickness of 2.5 nm. For the 16 nm AuNP the procedure was adapted from Lin *et al.*,[24] in which, initially, the amount of $KMnO_4$ was calculated to achieve the desired manganese dioxide layer thickness without precursor excess, considering the AuNP as spheres with an average diameter of 16 nm. The amount of $KMnO_4$ for each of the intended thicknesses is presented in Table 1. The values in Table 1 were obtained supposing that $HAuCl_4$ was converted entirely to AuNP, which is reasonable for the method described by Frens,[29] and that the AuNP were spherical with a diameter of 16 nm; from those considerations, and taking the gold density at room temperature (19.32 g cm^{-3}), the mass of a 16 nm radius spherical AuNP was calculated. The numerical concentration of nanoparticles and the volume of one AuNP was estimated. Subsequently, the radius of the MnO_2 shell was added to that of AuNP and, considering the volume of MnO_2 to form the overlayer and the density of MnO_2 (5.0 g cm^{-3}), the amount of MnO_2 necessary to cover each AuNP was determined from the numerical concentration of AuNP and, from that, the amount of $KMnO_4$ in the entries of Table 1. This procedure aimed to avoid that excess permanganate would still be present in the SHIN suspension. Oxalate ion reduced manganese(VII), so the concentration of oxalate was kept as a fifth of the permanganate concentration. To 10.0 mL of AuNP colloids, KOH (10.0 mmol L^{-1}) was added to adjust the pH to 9.5-10.0. After the pH adjustment, in an ice bath, one of the volumes presented in Table 1 of a 10.0 mmol L^{-1} $KMnO_4$ solution was added, followed by the corresponding volume of 10.0 mmol L^{-1} $Na_2C_2O_4$, to obtain a certain nominal MnO_2 thickness. After stirring for 10 min, the resulting suspension was introduced in a thermostatic bath at 60.0 °C for 2 h. After this time, the suspension changed from bright red to light purple in different degrees depending on the amount of $KMnO_4$ added.

Characterization of Au@MnO_2

The LSPR band of the Au@MnO_2 nanoparticles was measured in an Ocean Optics (Orlando, USA) USB2000 + XR1 + ES spectrometer with a light source in the 200-1800 nm range, using a 5 mm path-length quartz cell. The transmission electron microscopy (TEM) technique was used to characterize the size and shape of AuNP and Au@MnO_2. Additionally, STEM-HAADF experiments were performed to obtain a qualitative analysis of the elemental composition of the nanostructures. The electron microscopy experiments with energy dispersive spectroscopy (EDS) chemical analyses were performed in a transmission electron microscope FEI (Hillsboro, USA) Titan 80-300 using a 300 kV acceleration voltage.

SHINERS and SHINEF spectroscopic measurements

The SHINEF and SHINERS spectra from the probe molecule IR-820 were recorded on a Bruker (Billerica, USA) SENTERRA Raman spectrometer coupled to an Olympus BX51 optic microscope. A 50× objective (numerical aperture = 0.50) was used to acquire the Raman spectra. The experimental conditions for the SHINEF spectra were as follows: λ_0 = 785 nm, laser power of 25 mW, and 60 s for acquisition; for the SHINERS spectra, λ_0 = 633 nm, laser power of 10 mW, and 60 s spectral acquisition.

Table 1. Volumes of 10 mmol L^{-1} $KMnO_4$ and $Na_2C_2O_4$ solutions used for achieving different nominal thicknesses of MnO_2 over the Au nanoparticles (16 nm)

Nominal MnO_2 overlayer thickness / nm	0.8	1.2	2.5	3.5	5.0	10
Volume of 10.0 mmol L^{-1} $KMnO_4$ / μL	2.7	43.6	105.0	164.5	270.0	855.0
Volume of 10.0 mmol L^{-1} $Na_2C_2O_4$ / μL	0.54	8.7	21.0	32.9	50.0	171.0

Results and Discussion

Characterization of Au@MnO_2

The AuNP and Au@MnO_2 nanoparticles (using AuNPs 16 nm synthesized with 1000 µL of sodium citrate) were characterized by their LSPR position using UV-Vis spectroscopy. Figure 1 presents the extinction spectra of AuNP and the extinction spectra after reaction with different amounts of $KMnO_4$, which were expected to result in the deposition of MnO_2 ultrathin shells. One can observe in Figure 1 a red shift of the AuNP LSPR band as the amount of permanganate added to the AuNP suspension increased.

The shift was of around 1 nm for the Au@MnO_2 nanoparticles with a ca. 0.8 nm thick manganese oxide overlayer, and it was as high as 57 nm for ca. 10 nm oxide, which may also be due to the formation of clusters for higher permanganate concentrations. The shift of the LSPR band was an evidence of the formation of a MnO_2 overlayer on the AuNP, resulting in Au@MnO_2 and the increase in the MnO_2 shell thickness with the increase in MnO_4 available for reaction. Using UV-Vis spectroscopy as a diagnostic tool, it allowed quick monitoring of LSPR changes in Au@MnO_2. Using careful experimental protocols, the technique revealed a quite reproducible tendency in the LSPR spectra with an increasing MnO_2 overlayer thickness.

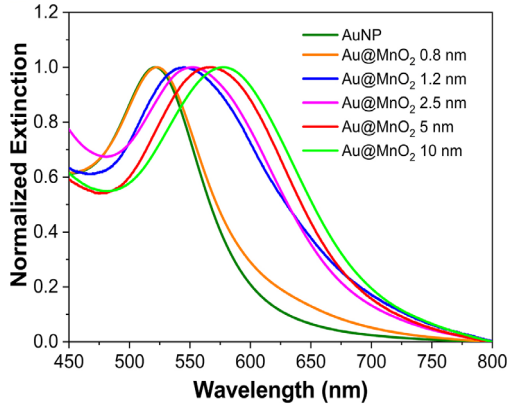

Figure 1. UV-Vis spectra of Au@MnO_2 core-shell nanoparticles for different shell thicknesses. All spectra have been normalized for the extinction at the top of the LSPR band.

TEM was used to ascertain the MnO_2 overlayer formation and morphology of Au@MnO_2 nanoparticles. TEM micrographs of Au@MnO_2 using AuNPs (50 nm) synthesized with 500 µL of sodium citrate are shown in Figure 2. It can be observed in Figure 2a that the AuNP, which was characterized by the sharp contrast to the background, is covered by a thin layer, indicated by a more diffuse contrast, assigned to the presence of manganese oxide. The high-resolution TEM image in Figure 2b presents the structure, where one may measure an interatomic distance of 2.3 Å (see zoom-in in Figure 2c), which is quite close to the interatomic distance in Au(111).[30] On the other hand, the overlayer has no different interlayer distance having an amorphous structure, which may be a result of the deposition procedure. The observation of this overlayer is indicative of effective coverage of the Au nanoparticles by the oxide.[19] EDS analysis gave further evidence that the overlayer on the AuNP is composed of manganese oxide, as shown in Figure 2d.

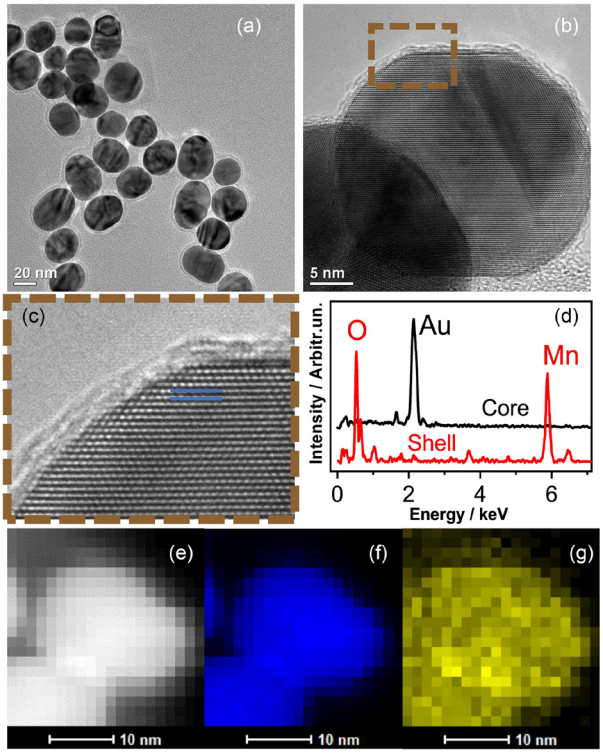

Figure 2. (a) and (b) different magnifications of TEM Au@MnO_2 (using Frens[29] 50 nm AuNP) with 2.5 nm thickness. (c) Digital zoom of (b) with Au interatomic distance measurement. (d) EDS spectrum confirms the core-shell-nanoparticle chemical composition. (e) Composite HAADF images of Au@MnO_2 (using Frens[29] 16 nm AuNP) with 2.5 nm thickness and the chemical image for (f) Au and (g) Mn.

Finally, as additional evidence for the core-shell structure, STEM/HAADF images were acquired for the material and are presented in Figures 2e-2g. One may notice that the composite image in Figure 2e and chemical images for Au and Mn (based on the spectra in Figure 2d) are presented in Figures 2f and 2g, respectively. The lateral resolution of the image is ca. 1.4 nm. The area occupied by the Au signal (Figure 2e) is smaller than the morphological image of the whole particle. On the other hand, the mapping for Mn (Figure 2g) indicates the presence of this element in an area similar to the composite image (Figure 2e), which suggests that there is an overlayer on the AuNP constituted of manganese oxide. It is also possible to estimate the thickness

of the manganese oxide layer based on the HAADF image as ca. 2.8 nm, evidenced by the difference between the Au and Mn images. The above result adds evidence to the formation of a core-shell structure Au@MnO_2.

SHINEF

The Au@MnO_2 materials prepared are potential substrates for SHINERS and SHINEF applications. In the present study, the indocyanine dye IR-820 was employed as a probe molecule because it presents pre-resonance Raman at 633 nm, which allows evaluating the SHINERS performance and using it as a fluorescence probe when excited at 785 nm.[26,31] The performance of the Au@MnO_2 nanoparticles (using AuNPs 16 nm synthesized with 1000 µL of sodium citrate) was evaluated for both SHINERS and SHINEF by the analytical enhancement factor AEF proposed by Le Ru *et al.*[22] (equation 1).

Fluorescence is expected to be suppressed in metallic surfaces such as the AuNP, which is an opposite behavior compared to the Raman scattering of molecules adsorbed on plasmonic nanostructures.[18] The fluorescence suppression in the presence of metallic surfaces (like AuNPs) is due to the energy transfer from the excited states of the fluorophore to the metallic structure so the radiative decay strongly loses intensity.[32,33] This way, for the occurrence of plasmonic enhancement of fluorescence, resulting in SEF, it is essential that there is a spatial gap between the metal and the fluorophore to decrease the probability of non-radiative energy transfer. On the other hand, the gap thickness has to be carefully controlled, so that there is a balance between the necessary distance fluorophore-surface but there still local field enhancement by the plasmonic excitation of the AuNP to increase the fluorescence intensity. The distance range most usually verified as the best for SEF in the literature is 5 to 10 nm.[18,20,21]

In the present study, the fluorescence spectra of IR-820 1.0×10^{-5} mol L^{-1} excited at 785 nm were obtained from the dye in contact with either AuNP or Au@MnO_2 with nominal thicknesses of 2.5, 5.0 and 10 nm, in the pursue of the best thickness for optimizing the SHINEF performance. Figure 3 presents the fluorescence spectrum of IR-820 and SEF/SHINEF spectra of IR-820 in the presence of AuNPs and AuNPs@MnO_2.

The fluorescence spectrum of IR-820 in direct contact with AuNPs in Figure 3 presented a sharp decrease in fluorescence intensity compared to the IR-820 solution. As can be observed in Table 2, the calculated AEF indicates 10 times decrease in intensity. Additionally, one may observe an increase in the IR-820 fluorescence intensity as the MnO_2 layer thickness increases from 2.5 to 5 nm, followed by an intensity decrease for the 10 nm thick MnO_2 layer; this result is translated into AEF in the entries of Table 2.

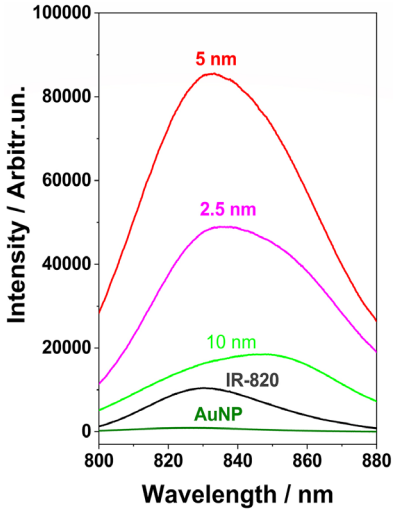

Figure 3. Fluorescence spectrum of IR-820 1.0×10^{-5} mol L^{-1} and SEF/SHINEF spectra of IR-820 in the presence of AuNPs and Au@MnO_2 with 2.5, 5.0, and 10 nm nominal MnO_2 thicknesses (λ_0 = 785 nm).

Table 2. SHINEF AEF for four different bands of the IR-820 spectra on Au@MnO_2 as a function of the nominal thickness of the manganese oxide overlayer, calculated according to equation 1, for the spectra excited at 785 nm

SHINEF AEF			
AuNP	2.5 nm	5 nm	10 nm
0.085	6.6	11.4	2.5

SHINEF AEF: shell-isolated nanoparticles enhanced fluorescence analytical enhancement factor.

In addition to the intensity variation, differences were also observed in the fluorescence spectral profile. The observed changes, which were both in maximum position and line width, may be result of the changes in the medium around the IR-820 fluorophore. The medium changes could interfere with those spectral characteristics due to the complexity of the plasmon-enhancement phenomenon.[20] However, some factors are usually the most important in the spectral profile of cyanine dyes like IR-820 and can strongly interfere in the spectral profile, such as the formation of dimers in higher concentrations, the adsorption geometry, and intensity of interaction between the dye and the MnO_2 surface.[34] To the above three factors may be attributed most of the variations observed in IR-820 SHINEF spectra, as it has been previously observed for IR-820 adsorbed on Ag@SiO_2.[31]

SHINERRS

Figure 4 displays the SHINERS spectra of IR-820 1.0×10^{-5} mol L^{-1} on Au@MnO_2 (using AuNPs 16 nm

synthesized with 1000 µL of sodium citrate) with several thicknesses of the manganese oxide overlayer and the Raman spectrum of an IR-820 solution in the same concentration, excited at 633 nm. It would be interesting to reinforce that the IR-820 dye is in pre-resonance with the 633 nm laser line so that the spectra obtained could be better described as 'shell-isolated nanoparticles enhanced resonance Raman scattering' (SHINERRS). The SHINERRS spectra obtained in the present study agree very well with the spectra of previous studies on the IR-820 dye,[26,31,35] which were interpreted as an indication of adsorption of the dye with the aromatic ring perpendicular to the surface and low interaction of the sulfonate groups with the metallic surface.

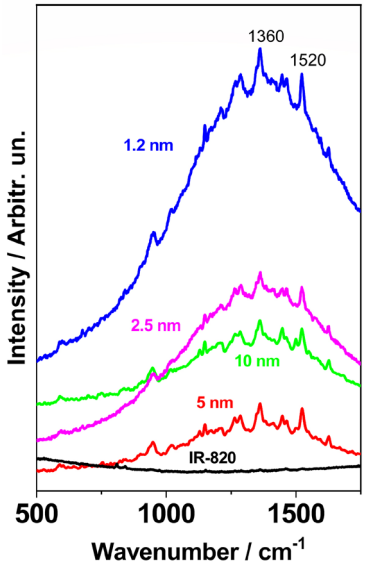

Figure 4. Raman spectra and SHINERS on $Au@MnO_2$ at different thicknesses, as shown in the figure, of IR-820 1.0×10^{-5} mol L^{-1} in solution.

It is also worth mentioning that $Au@MnO_2$ presented higher stability, both chemical and temporal when compared to non-protected AuNP. However, a trend that may be noticed in Figure 4 is that the Raman intensity of the IR-820 dye decreased with the MnO_2 overlayer thickness, which is a consequence of the increasing distance between the plasmonic nanoparticles and probe molecule. One may notice that there is no substantial decrease in the SHINERS intensity as the oxide layer thickens, as seen in Table 3. The SHINERS intensity decreases more markedly from 1.2 to 2.0 nm, but thicker layers present a fluctuation in SHINERS intensity. That may be attributed to the pre-resonant properties of the probe dye IR-820 excited at 633 nm.

The AEF for the SHINERRS spectra were calculated according to equation 1 and are presented in Table 3, using the band at 1520 cm^{-1}. The decrease in the Raman intensity may be explained by the decrease of the electromagnetic field by the fourth power of the distance between the Raman molecular probe and the plasmonic surface.[36] However, it should be noticed that the advantages of using a surface with different properties compared to gold may turn out to be advantageous depending on the application, even with the decrease in performance of the Raman enhancement. That would be the case in samples with a complex environment, such as dissolved salts or molecules, which could cause aggregation or coagulation of unprotected nanoparticles.

Table 3. SHINERS AEF for four different bands of the IR-820 spectra on $Au@MnO_2$ as a function of the thickness of the manganese oxide overlayer, calculated according to equation 1, for the spectra excited at 633 nm

υ / cm^{-1}	SHINERS AEF			
	1.2 nm	2.5 nm	5 nm	10 nm
1532	86	46	60	49

SHINERS AEF: shell-isolated nanoparticles enhanced Raman spectroscopy analytical enhancement factor.

The SHINERRS results evidence that the increasing distance between the adsorbate and the Au core strongly affects the scattering intensity. However, one may still observe a considerable enhancement even for the 10 nm MnO_2 layer. It should be reinforced that this study used moderated concentration, which increases the underestimation of the enhancement factor by the AEF method.

Conclusions

Gold nanoparticles coated with different manganese dioxide ultrathin overlayers were synthesized, varying the starting amount of manganese precursor permanganate to ensure that no excess of the precursors was present in the final product. The $Au@MnO_2$ materials were characterized by UV-Vis, high-resolution TEM, EDS, and STEM-HAADF techniques. The red shift of the AuNP LSPR band with the increasing amount of MnO_2 was a strong indication of the oxide coating and a qualitative evidence of the growing thickness of the shell. The layer with MnO_2 was confirmed by high-resolution TEM, EDS, and STEM-HAADF techniques.

$Au@MnO_2$ were used as substrates in SHINERS and SHINEF spectroscopies, using the probe molecule IR-820 dye, and calculating the AEF to compare different shell thicknesses. For SHINERS, the nanoparticles with a 1.2 nm layer presented the best performance, while for SHINEF nanoparticles with a 5.0 nm layer presented the best performance.

Acknowledgments

The authors thank FAPEMIG, CNPq, and CAPES (financing code 001) for financial support. GPO thanks CAPES for a fellowship. GFSA thanks CNPq for a research fellowship.

Author Contributions

Gabriela P. Oliveira was responsible for data curation, investigation, methodology, writing-original draft; Tatiana B. V. Neves for data curation, methodology, writing-review and editing; Linus P. F. Peixoto for formal analysis, methodology, writing-review and editing; Sandra M. Landi for formal analysis, methodology, writing-review and editing; Bráulio S. Archanjo for formal analysis, methodology, writing-review and editing; Gustavo F. S. Andrade for conceptualization, formal analysis, funding acquisition, supervision, writing-review and editing.

References

1. Petryayeva, E.; Krull, U. J.; *Anal. Chim. Acta* **2011**, *706*, 8. [Crossref]
2. Willets, K. A.; Van Duyne, R. P.; *Annu. Rev. Phys. Chem.* **2007**, *58*, 267. [Crossref]
3. Li, M.; Cushing, S. K.; Wu, N.; *Analyst* **2015**, *140*, 386. [Crossref]
4. Le Ru, E. C.; Etchegoin, P. G. In *Principles of Surface-Enhanced Raman Spectroscopy*, 1st ed.; Elsevier: Amsterdam, NL, 2009.
5. Toma, H. E.; Zamarion, V. M.; Toma, S. H.; Araki, K.; *J. Braz. Chem. Soc.* **2010**, *21*, 1158. [Crossref]
6. Fan, M.; Andrade, G. F. S.; Brolo, A. G.; *Anal. Chim. Acta* **2011**, *693*, 7. [Crossref]
7. Fan, M.; Andrade, G. F. S.; Brolo, A. G.; *Anal. Chim. Acta* **2020**, *1097*, 1. [Crossref]
8. Camacho, S. A.; Sobral-Filho, R. G.; Aoki, P. H. B.; Constantino, C. J. L.; Brolo, A. G.; *Analyst* **2017**, *142*, 2717. [Crossref]
9. Santos, J. J.; Toma, S. H.; Yatsuzuka, R. E.; Araki, K.; *J. Braz. Chem. Soc.* **2020**, *31*, 2274. [Crossref]
10. Guerrini, L.; Pazos-Perez, N.; Garcia-Rico, E.; Alvarez-Puebla, R.; *Cancer Nanotechnol.* **2017**, *8*, 5. [Crossref]
11. Jeong, Y.; Kook, Y.-M.; Lee, K.; Koh, W.-G.; *Biosens. Bioelectron.* **2018**, *111*, 102. [Crossref]
12. Peixoto, L. P. F.; Santos, J. E. L.; Andrade, G. F. S.; *Quim. Nova* **2019**, *42*, 1050. [Crossref]
13. Ding, S.-Y.; Yi, J.; Li, J.-F.; Ren, B.; Wu, D.-Y.; Panneerselvam, R.; Tian, Z.-Q.; *Nat. Rev. Mater.* **2016**, *1*, 16021. [Crossref]
14. Lu, L.; Zhang, J.; Jiao, L.; Guan, Y.; *Nanomaterials* **2019**, *9*, 916. [Crossref]
15. Santos, E. B.; Sigoli, F. A.; Mazali, I. O.; *J. Braz. Chem. Soc.* **2015**, *26*, 970. [Crossref]
16. Li, J. F.; Huang, Y. F.; Ding, Y.; Yang, Z. L.; Li, S. B.; Zhou, X. S.; Fan, F. R.; Zhang, W.; Zhou, Z. Y.; Wu, D. Y.; Ren, B.; Wang, Z. L.; Tian, Z. Q.; *Nature* **2010**, *464*, 392. [Crossref]
17. Li, J.-F.; Zhang, Y.-J.; Ding, S.-Y.; Panneerselvam, R.; Tian, Z.-Q.; *Chem. Rev.* **2017**, *117*, 5002. [Crossref]
18. Guerrero, A. R.; Aroca, R. F.; *Angew. Chem., Int. Ed.* **2011**, *50*, 665. [Crossref]
19. Anema, J. R.; Li, J.-F.; Yang, Z.-L.; Ren, B.; Tian, Z.-Q.; *Annu. Rev. Anal. Chem.* **2011**, *4*, 129. [Crossref]
20. Aroca, R. F.; Teo, G. Y.; Mohan, H.; Guerrero, A. R.; Albella, P.; Moreno, F.; *J. Phys. Chem. C* **2011**, *115*, 20419. [Crossref]
21. Aroca, R. F.; *Phys. Chem. Chem. Phys.* **2013**, *15*, 5355. [Crossref]
22. Le Ru, E. C.; Blackie, E.; Meyer, M.; Etchegoin, P. G.; *J. Phys. Chem. C* **2007**, *111*, 13794. [Crossref]
23. Rodrigues, D. C.; de Souza, M. L.; Souza, K. S.; dos Santos, D. P.; Andrade, G. F. S.; Temperini, M. L. A.; *Phys. Chem. Chem. Phys.* **2015**, *17*, 21294. [Crossref]
24. Lin, X.-D.; Uzayisenga, V.; Li, J.-F.; Fang, P.-P.; Wu, D.-Y.; Ren, B.; Tian, Z.-Q.; *J. Raman Spectrosc.* **2012**, *43*, 40. [Crossref]
25. Wang, T.; Le, Q.; Zhang, J.; Zhang, Y.; Li, W.; *Electrochim. Acta* **2017**, *253*, 311. [Crossref]
26. Marques, F. C.; Azevedo, G. C.; Senna, C. A.; Archanjo, B. S.; Corrêa, C. C.; Matos, R. C.; dos Santos, D. P.; Andrade, G. F. S.; *Spectrochim. Acta, Part A* **2022**, *272*, 120988. [Crossref]
27. Zhou, X.; Zhao, G.; Chen, M.; Gao, W.; Zhou, X.; Xie, X.; Yang, L.; Du, G.; *ACS Sustainable Chem. Eng.* **2018**, *6*, 3948. [Crossref]
28. Abdulrahman, H. B.; Kołątaj, K.; Lenczewski, P.; Krajczewski, J.; Kudelski, A.; *Appl. Surf. Sci.* **2016**, *388*, 704. [Crossref]
29. Frens, G.; *Nat. Phys. Sci.* **1973**, *241*, 20. [Crossref]
30. Gao, M.; Song, Y.; Liu, Y.; Jiang, W.; Peng, J.; Shi, L.; Jia, R.; Muhammad, Y.; Huang, L.; *Appl. Surf. Sci.* **2021**, *537*, 147912. [Crossref]
31. Neves, T. B. V.; Landi, S. M.; Sena, L. A.; Archanjo, B. S.; Andrade, G. F. S.; *RSC Adv.* **2015**, *5*, 59373. [Crossref]
32. Geddes, C. D.; Lakowicz, J. R.; *J. Fluoresc.* **2002**, *12*, 121. [Crossref]
33. Geddes, C. D.; *Metal-Enhanced Fluorescence*; John Wiley & Sons, Inc.: New Jersey, USA, 2010.
34. Hildebrandt, P.; Stockburger, M.; *J. Phys. Chem.* **1984**, *88*, 5935. [Crossref]
35. Neves, T. B. V.; Andrade, G. F. S.; *J. Spectrosc.* **2015**, *2015*, ID 805649. [Crossref]
36. Pieczonka, N. P. W.; Aroca, R. F.; *ChemPhysChem* **2005**, *6*, 2473. [Crossref]

Submitted: May 23, 2022
Published online: November 23, 2022